Biochimica et Biophysica Acta 1814 (2011) 102–110

Contents lists available at ScienceDirect

Biochimica et Biophysica Acta

journal homepage: www.elsevier.com/locate/bbapap

Review

# Application of AFM and optical biosensor for investigation of complexes formed in P450-containing monooxygenase systems

A.I. Archakov, Yu D. Ivanov *

*Institute of Biomedical Chemistry, Moscow, Russia*

ARTICLE INFO

*Article history:*
Received 6 May 2010
Received in revised form 20 August 2010
Accepted 29 August 2010
Available online 8 September 2010

*Keywords:*
Cytochrome P450
Optical biosensor
AFM

ABSTRACT

Atomic force microscopy (AFM) allows to visualize and count the individual protein molecules and their complexes within multiprotein systems. On the other hand, optical biosensor (OB) provides information on complex formation kinetics as well as complex lifetime ($\tau_{LT}$) and affinity. Comparison of complex lifetime $\tau_{LT}$ with the time required for enzyme's catalytic cycle ($\tau_{cat}$) enables to characterize productive complexes and distinguish them from non-productive ones. Both these approaches were applied for the analysis of the three cytochrome P450-containing monooxygenase systems: cytochrome P450 101, cytochrome P450 11A1 and cytochrome P450 2B4. By using AFM, the formation of binary and ternary protein complexes was registered in all the three systems. OB analysis enabled to kinetically characterize these binary and ternary complexes. It was shown that the binary complexes putidaredoxin reductase (PdR)/putidaredoxin (Pd) and Pd/cytochrome P450 101 (P450 101) formed within the P450 101 system and, also, the binary complexes adrenodoxin reductase (AdR)/adrenodoxin (Ad) and Ad/cytochrome P450 11A1 (P450 11A1) formed within the P450 11A1 system are non-productive (deadlock). At the same time, the ternary PdR/Pd/P450 101 and AdR/Ad/P450 11A1 complexes proved to be productive. The binary cytochrome P450 reductase (Fp)/cytochrome P450 2B4 (2B4) complexes and the ternary Fp/2B4/cytochrome b5 (b5) complexes formed within P450 2B4 system were productive.



## 1. Introduction

The enzymatic systems may be conventionally divided into two major groups: (I) single-protein self-sufficient systems (P450 102 [P450 BM3], P450 55 [P450nor], *etc.*) which do not require protein partners for the catalytic reaction to occur [1,2] and (II) more complicated, multiprotein systems (P450 101 [P450cam], P450 11A1 [P450scc], and P450 2B4 [P450LM2]) whose catalytic reactions involve protein partner interaction [3–6]. The information on the key enzyme's structure and its catalytic constant ($k_{cat}$) is very important for elucidation of the reaction mechanisms of (I) and (II) groups. At the same time, in case of group (II) additional information (data on protein complexes' structure and protein partners' interactions) is also of great importance.

Until recently, direct detection of protein complexes in enzymatic systems has been a challenging problem. As a rule, conclusions as to the occurrence of protein complex formation were made on indirect evidence: optical absorption measurements (*e.g.*, spin shift measurement in heme-containing proteins), resonance energy transfer fluorescence analysis, electrochemical data, *etc.* [7–9]. Formation of redox partners' complexes was mostly characterized based on their measured dissociation constant ($K_D$) [10]. However, detailed functional characterization of protein complexes required not only the knowledge of their $K_D$ but also the measurement of kinetic rate constants for complex formation and decay ($k_{on}$ and $k_{off}$). At the same time, characterization of redox partners' complexes – through direct determination of their $k_{on}$ and $k_{off}$ – presented serious difficulties. The knowledge of $k_{off}$ values is very important because it enables to calculate complex lifetime $\tau_{LT} = (k_{off})^{-1}$ and to compare this time with the time required for a single hydroxylation reaction cycle ($\tau_{cat}$) thereby estimating complex productivity. According to the present views, those complexes whose lifetime is sufficient for completion of one monooxygenase cycle and, consequently, for reaction product formation are productive; conversely, those of them whose lifetime is insufficient for completion of one such cycle and, hence, for reaction product formation are non-productive [11,12].

AFM and OB are nanotechnological label-free devices which, being used as a complementary system, may be considered as a powerful analytical tool to study protein–protein interactions. Inestimable advantages of AFM are its high concentration sensitivity and spatial resolution; these abilities of the method allow registering, visualizing and counting single macromolecules and their complexes. In its turn, OB enables to measure $k_{on}$ and $k_{off}$ for the complex formation reaction and complex lifetime $\tau_{LT}$ and its dissociation constant $K_D$. Combination of

* Corresponding author. Tel.: +7 495 246 3761; fax: +7 495 245 0857.
*E-mail address:* Yurii.Ivanov@rambler.ru (Y.D. Ivanov).

1570-9639/$ – see front matter © 2010 Elsevier B.V. All rights reserved.
doi:10.1016/j.bbapap.2010.08.013

AFM and the OB enables obtaining information as to the complexes' structure and their functional characterization in near-native conditions.

### 1.1. AFM for visualization and count of proteins and protein complexes

Nowadays, AFM – a rather new and fast-developing nanotechnology – is finding an increasing application. It enables to establish macromolecular structure with nearly as high a resolution as that from X-ray diffraction. The major advantages of AFM involve its abilities: (a) to conduct measurements in near-native conditions; (b) to visualize single macromolecules without labeling; (c) to provide information on the sizes and forms of protein complexes. Point (c) is worth highlighting. By now, the following sizes of individual proteins have been established using the X-ray and NMR methods: in the cytochrome P450 101 system, the sizes of P450 101 (3.3 nm × 5.6 nm × 5.7 nm), Pd (3.0 nm × 3.6 nm × 4.0 nm) and PdR (2.5 nm × 4.3 nm × 6.5 nm) [13–15]; in the P450 2B4-system, the sizes of P450 2B4 truncated (5.6 nm × 5.4 nm × 3.1 nm), cytochrome P450 reductase truncated (8.5 nm × 6.9 nm × 4.6 nm) and cytochrome b5 truncated (3.3 nm × 2.8 nm × 3.8 nm); (of note, for the P450 2B4 system only the sizes of truncated and not of full-length proteins were reported [16–18]; and in the P450 11A1 system, the sizes of Ad (3.8 nm × 3.4 nm × 4.4 nm) and AdR (5.8 nm × 5.4 nm × 4.0 nm) [19,20]. The structure of the membranous P450 11A1 still remains to be clarified. At the same time AFM easily enables to visualize both membrane and soluble proteins and their respective complexes. For example, by use of AFM technology the images of individual molecules of membrane full-length cytochromes P450 2B4 and P450 11A1, both incorporated into lipid layers, were obtained [21,22]. Therefore, AFM provides a rapid means for obtaining high-resolution images of biological macromolecules and appears to be a useful technology that complements the cryo-electron microscopy, X-ray and NMR technologies.

AFM-based registration scheme consists of AFM microscope and AFM-biochip with immobilized macromolecules [23]. The commonly used AFM measurement is based on the monitoring of cantilever's bending due to the interaction force emerging between the AFM tip of cantilever and the macromolecule immobilized onto atomically smooth support upon scanning [23–25]. High spatial resolution provided by AFM enables to detect, in a counting mode, a wide range of biological objects – single cells, single viruses, DNA and proteins – based on their sizes [26–35]. Of note, the vertical resolution of protein structure – obtainable by use of AFM technology – constitutes 0.1–0.2 nm, while the lateral one is somewhat lower (~0.5 nm) due to a tip-related effect [23]. Therefore, the height of imaged protein appears to be a basic measure of its size. In most cases, the heights of protein complexes exceed those of their constituent proteins. Thus, the heights of protein objects may serve as a valid criterion for distinguishing between the monomeric proteins and protein complexes [36–41].

Analysis of distribution density with height ρ(h) for AFM-imaged proteins can be approximated by Eq. (1) [42]:

$$\rho(h) = \Sigma K_i \times \frac{(h-m_i)^2}{b_i^2} \times \exp\left[\frac{-(h-m_i)^2}{2b_i^2}\right], \quad (1)$$

where $K_i$, $m_i$, $b_i$ are the fitting parameters of $\rho(h)_i$ distribution. The heights of proteins can be determined as heights for corresponding distributions maximums ρ(h) of proteins as was shown for the putidaredoxin reductase [42].

The limitations of AFM technology are these: (a) low scan rate of the chip surface for commercially available AFMs; (b) the height of protein image could be somewhat less than the one from X-ray or NMR due to the molecule's deformation by AFM probe [39].

### 1.2. Optical biosensor for measuring complex formation kinetic parameters

Nowadays, OB nanotechnology for functional characterization and measuring of $k_{on}$ and $k_{off}$ is widely accepted [43–69]. OB allows direct detection of the target protein without the need of additional labeling. A high concentration detection limit (DL) was achieved for OBs ~ $10^{-12}$ M in real-time operation [70]. In addition, the throughput of these biosensors can be increased by the use of multichannel array format as was demonstrated for commercial 400-channel BIAcore Flexchip, designed for carrying out 400 analyses simultaneously (http://http://www.hvd.ru/p/p28.html). The most interesting label-free devices are based on surface plasmon resonance (SPR) and resonant mirror (RM) structures [62–67,71,72]. They are able to operate in real time thereby generating detailed information on the interaction parameters including: (a) the monitoring of kinetics for complex formation/decay reactions in real time for protein/protein, oligonucleotides/oligonucleotides, protein/lipid, and, also, drug/receptor interactions; (b) the simultaneous measurement of the association and dissociation rate constants ($k_{on}$ and $k_{off}$) for these reactions as well as calculation of the complex dissociation constant ($K_D = k_{off}/k_{on}$) and complex lifetime $\tau_{LT} = k_{off}$.; (c) the calculation of Gibbs free energy ($\Delta G$), enthalpy change ($\Delta H$) and entropy change ($\Delta S$) for complex formation reaction [51,54,68].

All proteins have the same refractive index and, since there is a linear correlation between resonance angle shift and surface protein concentration, the protein concentration changes due to protein–protein binding can be measured accurately. It is to be noted that optical biosensor is only able to register formation of protein complexes near the surface — at a distance within several hundred nanometers and not in the whole volume of the reaction mixture.

The association/dissociation rate constants can be determined using Fastfit program [73] that describes the experimental association curve by the exponential equation:

$$R = R_0 + R_f^* \left\{1 - exp\left(-\left(k_{on}C + k_{off}\right)^* t\right)\right\}, \quad (2)$$

where R is the response of the device, t is time, $R_0$ is the initial level of the signal (R at t = 0), C is the ligate concentration, and $R_f$ is the level of the signal in the equilibrium state (at t = ∞) — relative to the initial signal.

The OB technology has limitation: covalent immobilization of proteins through its positively charged amino acid residues on carboxymethylated dextran surface of the OB chip leads to blockage of these residues. Therefore, to clarify participation of protein amino acid residues in complex formation, each of the partners has to be alternatively immobilized, through these residues, on the dextran layer of OB cuvette.

### 1.3. OB-based approach for estimation of complex productivities

In a multiprotein enzymatic system, the following two relations between complex lifetime and the time of enzyme's catalytic cycle may be realized: the complex lifetime may be either shorter or longer than the catalytic cycle time, i.e. ($\tau_{LT} < \tau_{cat}$) or ($\tau_{LT} > \tau_{cat}$), respectively. The (OB-measured) lifetime of binary and ternary complexes formed within such a system may be used as a criterion for complex efficiency, i.e. its involvement in catalysis. Fig. 1 features two mechanisms, schematically illustrating the function of three-protein systems within each of which the intermediate protein C provides the relation between the other two proteins, A and B (such interaction is exemplified by ferrodoxin which acts by transferring electrons from the reductase to cytochrome P450 within the P450 101 and the P450 11A1 systems). The former mechanism is described by the shuttle model [74,75] and the latter, by the cluster model [76]. It should be

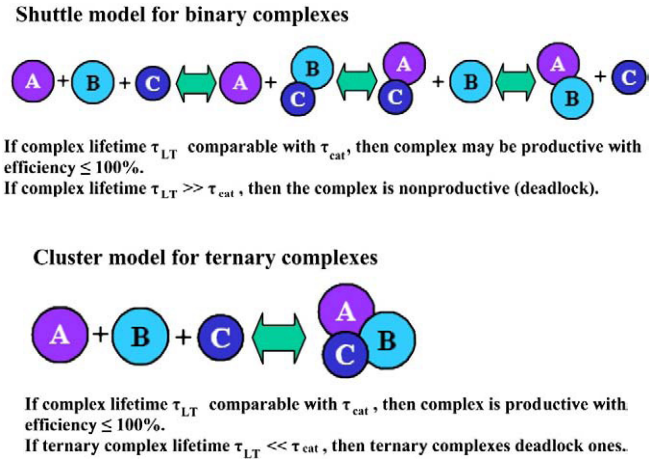


**Fig. 1.** Two models of functioning of three component (A, B, and C) protein systems. Turnover time $\tau_{cat} = 1/\tau_{cat}$ and complex lifetime $\tau_{LT} = 1/k_{off}$.

noted in this context that formation of complexes occurs, schematically, not only between A and C but, also, between B and C. Formation of A/B complexes was registered, for instance in the P450 101 system (PdR/P450 101), by use of AFM and OB, and in the P450 11A1 system (AdR/P450 11A1), by use of OB, on the surface of appropriate chips [11,12,40].

Consider the shuttle model for case (1) — where $\tau_{LT} < \tau_{cat}$. According to the shuttle model, the realization of a catalytic cycle is characterized by initial formation of the binary A/C complex which rapidly dissociates — whereupon the binary C/B complex is formed. In this situation, the binary complexes thus formed are actively involved in the catalytic cycle and may be considered as productive.

Now, consider the shuttle model for case (2) where the binary complex lifetime exceeds the time of a catalytic cycle ($\tau_{LT} > \tau_{cat}$). For simplicity, let us assume that $\tau_{LT} \gg \tau_{cat}$. In considering case (2), the following 3 requirements must be met: (i) the obligatory involvement of the 3rd (intermediate) protein C in providing electron transfer between proteins A and B if direct electron transfer between them is impossible; (ii) the shorter time of a catalytic cycle compared to the lifetime of C-including binary complexes; (iii) the impossibility (as presupposed by the shuttle model) of the ternary A/C/B complex formation on the basis of the (already formed) A/C complex with the 3rd partner, B. The shuttle model implies that the binary A/C complex cyclically dissociates with formation of the binary B/C complex and its subsequent dissociation.

However, the much too long complex lifetime vs. the time of a catalytic cycle excludes such a process. It appears, therefore, that such complexes are inefficient in realization of a catalytic cycle and may well be considered as non-productive (deadlock).

Symbolically, the efficiency of such complexes is expressed by Eq. (3):

$$Pr \sim \left\{ \left[ n\tau_{LT(A/C)}/\tau_{cat} \right]^{-1} \text{ or } \left[ n\tau_{LT(C/B)}/\tau_{cat} \right] \right\} * 100\%, \quad (3)$$

where Pr is productivity, $\tau_{LT\,(A/C)}$ and $\tau_{LT\,(C/B)}$ are A/C and C/B complex lifetimes, respectively, and symbol (n) indicates the number of associations/dissociations of binary complexes in the course of shuttle-mechanism realization.

If $\tau_{LT} \gg \tau_{cat}$, *e.g.* $\tau_{LT} \sim 100\tau_{cat}$, then Pr ~ 1%; in this case, such binary complexes are practically non-productive.

Now consider the cluster model in cases where a three-protein system may generate both binary and ternary complexes. Take case (1) where $\tau_{LT} > \tau_{cat}$ (for simplicity, let us assume, in particular, that $\tau_{LT} \gg \tau_{cat}$). Realization of the catalysis process within a long-lived complex occurs efficiently, if the 3rd redox partner would couple to the previously formed long-lived binary complex which has not enough time to dissociate in the framework of a catalytic cycle. Clearly, in such a situation, a ternary complex is bound to be formed. With the cluster model, such a ternary complex is productive if its lifetime is equal to or larger than the hydroxylation cycle time.

Thus, the efficiency of ternary complexes for the cluster model may be estimated in the two cases:

$$\text{Case(1)—where } (\tau_{LT} > \tau_{cat}) : Pr = 100\% \quad (4-1)$$

$$\text{Case(2)—where } (\tau_{LT} < \tau_{cat}) : Pr = \tau_{LT}/\tau_{cat} * 100\% \quad (4-2)$$

The aim of the present review was to demonstrate the abilities of the AFM and OB and summarize the available data on applications of the two devices for the revelation and functional characterization of complexes formed within the three-protein cytochrome P450-containing monooxygenase systems – P450 101, P450 11A1 and P450 2B4 – representing the three types of the P450 superfamily. Constituent components of the cytochrome P450 101 system are water-soluble proteins, PdR, Pd and P450 101; the cytochrome P450 11A1 system consists of two (soluble in the matrix) proteins, AdR and Ad which are associated with the inner membrane of mitochondria and the membrane-bound P450 11A1 protein [2]. The P450 2B4 system is a membrane-bound one, i.e. its partner proteins are each incorporated into the phospholipid membrane via their hydrophobic fragments [4]. The operation of the first two systems is realized through sequential transfer of two electrons from the reductase to P450 via the intermediate protein: either Pd or Ad. With the P450 2B4 system, two electrons are transferred sequentially from NADPH cytochrome P450 reductase (Fp) to P450 2B4 (2B4), or one electron is supplied by Fp while the other is supplied by cytochrome b5 (b5) [4].

The review demonstrates that AFM technology enables to observe not only binary but also ternary protein complexes in all the three cytochrome P450 systems. OB enables to measure kinetic constants of these complexes and their lifetimes. Based on OB data, it was shown that the binary PdR/Pd and Pd/P450 101 complexes and the binary AdR/Ad and Ad/P450 11A1 complexes formed within the P450 101 and P450 11A1 systems, respectively, had the much longer lifetimes ($\tau_{LT}$) than the time required for the single catalytic cycle ($\tau_{cat}$) completion. Therefore these complexes were non-productive (deadlock). At the same time, PdR/Pd/P450 101 and AdR/Ad/P450 11A1 ternary complexes formed within both these systems and characterized with lifetimes exceeding $\tau_{cat}$ proved to be productive. With the membranous P450 2B4 system, the binary Fp/2B4 and b5/2B4 and ternary Fp/2B4/b5 complexes were also productive.

## 2. AFM and OB for revelation and kinetic characterization of complexes within P450 systems

### 2.1. Cytochrome P450 101 system

#### 2.1.1. AFM in studies of the P450 101 systems

To obtain images of the system's individual proteins and their complexes, the appropriate solutions and mixtures were deposited on the AFM mica chips; then they were incubated — so as to allow the proteins and their complexes to be adsorbed and immobilized onto the AFM chip surface. After that, AFM chips were washed in ultrapure water to remove salts remnants. AFM images were obtained upon scanning of the AFM chip in air at the relative humidity 60–70% (with this humidity, the mica surface gets covered with a water layer; therefore, the protein molecules under study remain hydrated throughout [77]). AFM allowed to visualize the individual proteins PdR, Pd and P450 101 on mica and measure their heights [40]. The heights of proteins were estimated as $2.6 \pm 0.3$ nm (P450 101), $2.0 \pm 0.3$ nm (Pd) and $2.8 \pm 0.3$ nm (PdR) [40]. The fact that the actual sizes of proteins are somewhat less than those obtained by X-ray or NMR is explained by the molecule's contraction due to probe force.

In [40], the binary PdR/Pd, Pd/P450 101 and PdR/P450 101 complexes were identified according to their characteristic heights ($4.9 \pm 0.3$ nm, $4.3 \pm 0.3$ nm and $5.1 \pm 0.3$ nm) which were greater than those of single proteins.

Along with the binary complexes, the ternary PdR/Pd/P450 101 complexes were also registered [40]. Accordingly, the characteristic heights of ternary PdR/Pd/P450 101 complexes (in the range 6.5–9.5 nm) were greater than those of binary complexes.

#### 2.1.2. OB in studies of the P450 101 system

Formation of binary Pd/PdR, Pd/P450 101 and PdR/P450 101 complexes occurred within the P450 101 system upon Pd immobilization (Pdim) and did not occur within this system upon PdR or P450 101 immobilization — as was demonstrated in O-resonant mirror (OB-RM) experiments [78]. This means that the positively charged amino acid residues of PdR or P450 101 are absolutely necessary for their complexation with Pd. Comparison of the lifetime $\tau_{LT}$ of the binary Pd/PdR and Pd/P450 101 complexes in oxidation conditions with the time required for a single hydroxylation cycle $\tau_{cat}$ has shown that $\tau_{LT}$ of the two complexes is several times longer than their $\tau_{cat}$ [78]. The recently published data on the Pd binding potential has been the subject of much discussion. Some authors believe that reduced Pd binds to oxidized P450 101 at least 100 times more tightly compared to oxidized Pd [79]. Therefore to estimate the influence of proteins' oxidation state on their interaction kinetics, the kinetic constants ($k_{on}$ and $k_{off}$) and the dissociation constant $K_D$ were measured not only in oxidation conditions but also in hydroxylation conditions on a two-channel RM-OB (IAsys+) [12,80]. Since the association and dissociation of protein complexes in hydroxylation conditions are complicated processes, the complex formation processes were characterized by effective constants calculated according to Eqs. (2–3). The results of measurements are presented in Table 1.

Comparison of thermodynamic constants obtained in hydroxylation (*HYD*) and oxidation (*OX*) conditions showed that $K_D$ values for all the binary and ternary complexes are similar. Such constants for binary $Pd_{im}$/P450 101 complexes as $k_{off}$ and $\tau_{LT}$ are in the same order ($\tau_{LT} = 33 \pm 15$ s [*HYD*] and $17 \pm 9$ s [*OX*]); however, the $k_{off}$ and $\tau_{LT}$ for binary $Pd_{im}$/PdR complexes differ greatly: thus, $k_{off}$ of these complexes is 3.5 times higher while $\tau_{LT}$ is 3.5 times shorter in hydroxylation vs. oxidation conditions ($\tau_{LT} = 70 \pm 15$ s [*HYD*] and $256 \pm 66$ s [*OX*]). For P450 101/PdR complexes all the parameters in hydroxylation and oxidation conditions differ significantly; $\tau_{LT}$ in hydroxylation conditions is by one order longer than in oxidation conditions ($\tau_{LT} = 700 \pm 100$ s and $25 \pm 6$ s, respectively). Bearing in mind that $\tau_{cat} = 0.03$ s [81], it appears that the lifetime of every binary Pd/PdR or Pd/P450 101 complex exceeds by 2–3 orders the time required for completion of the catalytic cycle. As is known, direct electron transfer from PdR to P450 101 is prohibited and the realization of a single hydroxylation cycle requires the sequential transfer of 2 electrons from PdR to Pd and from Pd to P450 101 [4]. The efficiency of binary complex productivity calculated by Eq. (3) according to the shuttle model, is less than 0.1%. It appears therefore that the binary Pd/PdR and Pd/P450 101 complexes are practically non-productive and Pd not be able to act as an electron carrier from one binary complex to another; so, in this case the shuttle mechanism is apparently in action.

In [78] the formation of ternary PdR/Pd/P450 101 complexes in oxidation conditions based on OB-RM data was reported. Also, the formation of ternary PdR/Pd/P450 101 complexes in hydroxylation conditions was registered [12,80]. Formation of ternary PdR/Pd/P450 101 complexes occurred when P450 101 was added to the Pdim — in the presence of PdR brought up to saturation point. The lifetime of ternary complexes obtained in hydroxylation conditions ($\tau_{LT} = 2 \pm 1$ s) is essentially the same as in oxidation conditions. Therefore, based on Eqs. (4-1)–(4-2), it can be concluded that productivity of these complexes is 100%. In one such complex ~70 catalytic cycles may be realized.

Thus, AFM allows the registration and visualization of isolated proteins as well as of binary and ternary complexes within the P450 101 system whereas OB is able to measure the kinetic constants of complex formation processes, estimate the degree of productivity of ternary PdR/Pd/P450 101 complexes and establish the non-productivity of binary Pd/PdR and P450 101 complexes.

### 2.2. Cytochrome P450 2B4 system

#### 2.2.1. AFM in studies of the P450 2B4 system

The AFM technology enables to distinguish protein complexes from isolated proteins more easily if these complexes are formed from monomeric proteins or if one of the proteins occurs in solution as a monomer rather than an aggregate. This situation is observed more often for water-soluble proteins. The problem the researcher is faced with is that membrane proteins would form aggregates upon their solubilization. To obviate this problem, prior to AFM measurements, the lipid-free monomerization procedure of protein oligomers in buffer solution has to be conducted [41].

The approach for obtaining the AFM images of isolated membrane proteins Fp, 2B4 and b5 and their complexes involved monomerization procedure in solution with the use of Emulgen 913 at the first step followed by AFM registration and count of proteins at the second step [41]. As was demonstrated, in the course of this procedure the membrane proteins become monomers while retaining their activity [82,83]. Thus, the separately located Fp, 2B4 and b5 with the heights $2.2 \pm 0.2$ nm, $2.3 \pm 0.2$ nm and $1.8 \pm 0.1$ nm, respectively, were visualized. The binary Fp/2B4 and 2B4/b5 complexes were higher than isolated proteins: their characteristic heights were in the height range over 2.7 nm, with respective local maximums of $3.4 \pm 0.2$ nm and $2.8 \pm 0.2$ nm [41]. No formation of Fp/b5 complexes was registered [41]. The ternary Fp/2B4/b5 complex heights were found to be in the height range 4.3–6.2 nm [41].

#### 2.2.2. OB in studies of the P450 2B4 system

Earlier it was demonstrated that the P450 2B4 system, containing the monomerized membrane proteins 2B4, Fp and b5, was unable to form Fp/b5 complexes in oxidation conditions upon alternative immobilization of these proteins on OB-RM chips [72]. At the same time, the interprotein electron transfer between Fp and b5 with the rate constant $k = 0.4 \pm 0.1\ s^{-1}$ does occur [72]. The data were interpreted as indicating that the interprotein electron transfer for the Fp/b5 pair occurs through random collisions. The formation of complexes between Fp and 2B4 as well as between b5 and 2B4 in oxidation conditions was reported in [72]. The measured $k_{on}$ and $k_{off}$

**Table 1**
$k_{on}$, $k_{off}$, $K_D$, and lifetime ($\tau_{LT}$) of redox partners' complexes in the, P450 101, P450 11A1 and P450 2B4 systems [12,80].

| Pair | $k_{on}$ $10^4$, $(M*s)^{-1}$ | $k_{off}$ $10^{-3}$, $s^{-1}$ | $K_D$ $10^{-6}$, M | $\tau_{LT}$, s |
|---|---|---|---|---|
| $Pd_{im}$/PdR (*hyd*) | 0.45 ± 0.15 | 14 ± 3[a] | 3.4 ± 1.7 | 70 ± 15[a] |
| $Pd_{im}$/PdR (*ox*) | 0.35 ± 0.2 | 3.9 ± 1.0[a] | 1.1 ± 0.9 | 256 ± 66[a] |
| $Pd_{im}$/P450 101 (*hyd*) | 0.2 ± 0.1 | 30 ± 15 | 15 ± 15 | 33 ± 15 |
| $Pd_{im}$/P450 101 (*ox*) | 0.54 ± 0.4 | 60 ± 30 | 11 ± 14 | 17 ± 9 |
| P450 $101_{im}$/PdR (*hyd*) | 0.72 ± 0.12[a] | 1.4 ± 0.2[a] | 1.9 ± 0.6 | 700 ± 100[a] |
| P450 $101_{im}$/PdR (*ox*) | 0.014 ± 0.002[a] | 40 ± 10[a] | 2.9 ± 1.1 | 25 ± 6[a] |
| Ternary complexes | | 500 ± 200 | | 2 ± 1 |
| PdR/$Pd_{im}$/P450 101 (*hyd* and *ox*) | | | | |
| Fp/2B4 (*hyd*) | 1.3 ± 0.5[a] | 50 ± 20 | 0.26 ± 0.13 | 20 ± 8 |
| Fp/2B4 (*ox*) | 10 ± 3[a] | 140 ± 60 | 0.71 ± 0.37 | 7 ± 3 |
| b5/2B4 | 120 ± 50 | 0.4 ± 0.2 | 0.3 ± 0.2 | 3 ± 2 |
| Fp/b5 | No | No | No | No |
| Ternary complexes | | 200 ± 80 | | 5 ± 2 |
| Fp/b5/2B4 (*hyd*) (*ox*) | | 333 ± 111 | | 3 ± 1 |
| $Ad_{im}$/AdR (*hyd*) | 0.18 ± 0.04 | 2.0 ± 0.7 | 1.2 ± 0.6 | 500 ± 175 |
| $Ad_{im}$/AdR (*ox*) | 0.06 ± 0.02 | 3.5 ± 1.5 | 6 ± 4 | 286 ± 123 |
| $Ad_{im}$/P450 11A1 (*hyd*) | 0.7 ± 0.3[a] | 8.0 ± 2.0[a] | 1.1 ± 0.8[a] | 125 ± 30 |
| $Ad_{im}$/P450 11A1 (*ox*) | 5 ± 0.5[a] | 1.1 ± 0.1[a] | 0.022 ± 0.004[a] | 900 ± 80 |
| $AdR_{im}$/P450 11A1 (*hyd*) | 2.2 ± 0.4 | 10 ± 2 | 0.5 ± 0.2 | 100 ± 20 |
| $AdR_{im}$/P450 11A1 (*ox*) | 3.5 ± 0.7 | 11 ± 2 | 0.3 ± 0.15 | 90 ± 16 |
| P450 $11A1_{im}$/AdR (*hyd*) | 0.3 ± 0.1 | 40 ± 10 | 13 ± 8 | 25 ± 6 |
| P450 $11A1_{im}$/AdR (*ox*) | 0.3 ± 0.1 | 25 ± 5 | 8 ± 4 | 40 ± 8 |
| Ternary complexes | | 40 ± 20 | | 25 ± 13 |
| AdR/Ad/P450 11A1 (*hyd* and *ox*) | | | | |

[a] Statistically significant differences.

for the Fp/2B4 and b5/2B4 pairs showed no dependence on the protein partners' immobilization order. It appears that in case of membrane proteins the positively charged amino acid residues of 2B4, Fp and b5 do not play an essential role in complex formation. Thus, with the P450 2B4 system the hydrophobic interactions play a dominant role in protein complex formation — in contrast to the water-soluble P450 101 system.

To estimate the influence of the of proteins' oxidation state on their interaction constants, we have measured the $k_{on}$, $k_{off}$, $K_D$ and $\tau_{LT}$ not only in the oxidation but also in hydroxylation conditions [12,80]. The obtained results are presented in Table 1. It was found that Fp/b5 protein pairs would not form complexes upon their alternative immobilization either in hydroxylation or in oxidation conditions. The Fp/2B4 complexes were registered and their lifetimes were estimated in both conditions: $\tau_{LT} = 20 \pm 8$ s [*HYD*] and $\tau_{LT} = 7 \pm 3$ s [*OX*]. The ratio of complex lifetime ($\tau_{LT} = 20$ s) to the time required for the single catalytic cycle of benzphetamine N-demethylation ($\tau_{cat} = 11 \pm 2$ s) [72] shows that during complex lifetime the turnover number of the catalytic hydroxylation cycles was $\tau_{LT}/\tau_{cat} = 20/11 = \sim 2$. Therefore, according to Eqs. (4-1)–(4-2), the productivity (Pr) of Fp/2B4 complexes is 100% and in one such complex 2 catalytical cycles may be realized.

It was shown that in the presence of the third protein (b5) within the P450 2B4 system, the benzphetamine N-demethylation rate may increase up to 7.1 ± 0.5 s [72]. Also, the formation of ternary complexes between the oxidized forms of Fp, 2B4 and b5 was demonstrated [72]. In addition, the ternary Fp/2B4/b5 complexes were registered in both the hydroxylation and oxidation conditions when b5 was added to the $2B4_{im}$ chip in the presence of Fp brought up to saturation point [12]. Ternary Fp/2B4/b5 complexes had similar lifetimes in both conditions: $\tau_{LT} = 5 \pm 2\ s^{-1}$ [*HYD*] and $\tau_{LT} = 3 \pm 1\ s^{-1}$ [*OX*] (Table 1). The $\tau_{LT}/\tau_{cat}$ ratio was calculated and made up $\tau_{LT}/\tau_{cat} = (5 \pm 2)/7 \sim 1$. This means that the lifetimes of ternary complexes are sufficient to permit completion of one hydroxylation cycle. Therefore, according to Eqs. (4-1)–(4-2), all ternary complexes are productive.

Thus, AFM allows to register and visualize isolated proteins, binary Fp/2B4 and b5/2B4 complexes and ternary Fp/2B4/b5 complexes within the P450 2B4 system while OB is able to kinetically characterize and estimate the productivity of binary and ternary complexes thus formed. Application of the two methods did not allow to register formation of Fp/b5 complexes either in oxidation or hydroxylation conditions.

### 2.3. Cytochrome P450 11A1

#### 2.3.1. AFM in studies of the P450 11A1 system

The previously described AFM approaches, taken to study the water-soluble cytochrome P450 101 and the membrane-bound cytochrome P450 2B4, can also be applied to studying the mixed cytochrome P450 11A1 system that contains both water-soluble and membrane-bound protein types. The membranous P450 11A1 is able to form oligomers upon solubilization [4]. To solve the aggregation problem and be able to conduct AFM measurements within the P450 11A1 system, it was necessary to resort to monomerization procedure. In this study, to monomerize P450 11A1, we employed 12% Emulgen 913 — as in case of the P450 2B4 system.

At first the control AFM experiments on the influence of detergent on AFM images were conducted. For this purpose, we have obtained the images on mica that was first incubated in buffer solution (PBS), containing appropriate concentrations (C = 0 and C = 12%) of Emulgen 913, and then washed in distilled water. The sizes of non-specific objects on mica did not exceed 1 nm in both cases. To obtain additional data on the influence of detergent on measured protein heights, the control experiment on measuring the protein height was carried out with Ad monomers in buffer solution at both Emulgen concentrations (C = 0 and C = 12%). The control demonstrated that protein heights were equal in both conditions.

The AFM images of monomerized and non-monomerized CYP11A1 (12% and 0% Emulgen 913, respectively) are presented in Fig. 2. One can see that AFM images of monomerized proteins have lower heights than non-monomerized ones. The ρ(h) distribution of imaged objects with heights (Fig. 2) for non-monomerized P450 11A1 is well approximated by the sum of two curves according to Eq. (1). Heights of imaged objects with distribution maxima $\rho(h)_{1a}$ and $\rho(h)_{2a}$ are observed at $h_{max1a} = 2.4 \pm 0.3$ nm and at $\rho(h_{max})_{2a} = 3.8 \pm 0.4$ nm, respectively. At the same time, upon CYP11A1 monomerization in 12% Emulgen 913, the approximation of ρ(h) distribution is represented as the sum of two distributions: $\rho_1(h)$ with $h_{max1} = 1.6 \pm 0.2$ nm (share of imaged objects, 80%) and $\rho_2(h)$ with $h_{max2} = 2.6 \pm 0.3$ nm (share of imaged objects, 20%).

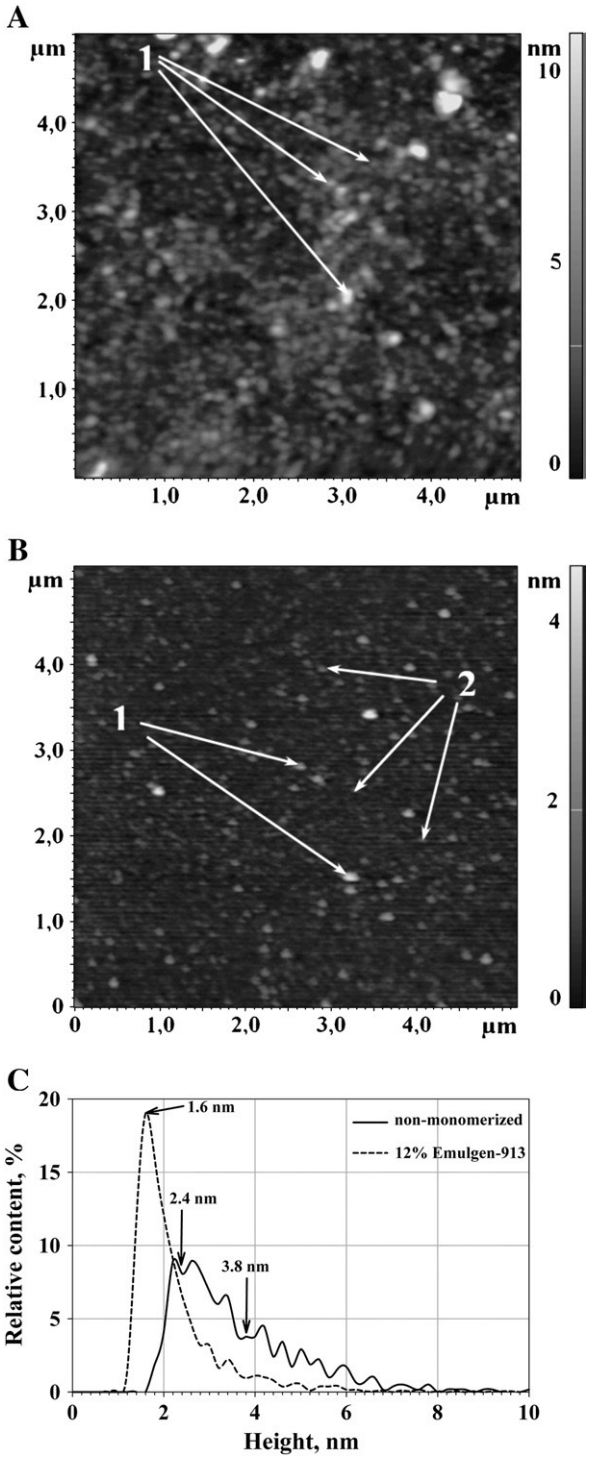


**Fig. 2.** AFM images of non-monomerized (A) and Emulgen 913-monomerized (B) CYP11A1 molecules and density of distribution (ρ(h)) with height of non-monomerized and monomerized CYP11A1 (C). AFM tapping mode. Experimental conditions: 100 μM CYP11A1 non-monomerized and 100 μM CYP11A1 monomerized in 50 mM KP, pH 7.4, containing 12% Emulgen 913 were diluted to obtain 1 μM of CYP11A1 in 50 mM KP with 0.5% Emulgen 913, pH 7.4, and immediately placed onto mica surface and left for 3 min. Then each sample was rinsed with distilled water. T = 25 °C. Arrows (1) indicate the images of CYP11A1 aggregates; arrows (2) indicate the images of CYP11A1 monomers [84]. The scan size was 5*5 $\mu m^2$; in total, 30 scans were analyzed in 3 experiments. Analysis of images was performed using the GRF program for calculation of object heights and for construction of a histogram for distribution of objects with heights (www.soft.ibmc.msk.ru). The monomerization scheme was as follows: to 2 μl of stock solution containing CYP11A1 (100 μM) in 50 mM KP, pH 7.4, was added 1.3 μl of 30% Emulgen 913 at T = 22 °C. The final concentration of Emulgen 913 in solution was brought to the required 12%. The mixture thus obtained was incubated at room temperature (22 °C) for 10 min [84].

Given that AFM images of 2B4 monomers have essentially the same size, 2.2 ± 0.2 nm [41] and molecular mass $M_r$ (2B4) ≈ $M_r$ (*CYP11A1*), it is reasonable to suggest that AFM images of monomerized protein with the smaller size ($h_{max1}$ = 1.6 ± 0.2 nm) correspond to the distribution of P450 11A1 monomers, while the AFM-imaged objects with the larger $h_{max2}$ = 2.6 ± 0.3 nm correspond to P450 11A1 oligomers. The fact that the sizes of P450 11A1 ($h_{max1}$ = 1.6 ± 0.2 nm) are somewhat less than expected is probably explained by the molecule's contraction due to AFM probe force.

Interestingly, the results of control to confirm the monomeric CYP11A1 activity have shown that the monomeric CYP11A1 is capable of converting 7-dehydrocholesterol to 7-dehydropregnenolone with $V_{max}$ = 0.48 ± 0.02 nmol/min/nmol CYP11A1 and $K_M$ = 0.32 ± 0.06 M. Both the $V_{max}$ values and the Ad-dependent $K_M$ values, as determined using monomeric CYP11A1, did not reveal significant differences compared with the oligomeric enzyme for which these values were $V_{max}$ = 0.51 ± 0.04 nmol/min/nmol and $K_M$ = 0.47 ± 0.15 M. Thus, the activity assays have demonstrated that the monomerization procedure does not significantly alter the functionality of CYP11A1 [84].

Distributions of imaged AdR and Ad with height ρ(h) are represented in Fig. 3. Analysis of these distributions shows that the majority (about 90%) of AdR images have the height of about 1.4–2.2 nm for which the distribution maxima ρ(h) are observed at $h_{max}$ = 1.8 ± 0.2 nm, while the height of a typical Ad image is about 0.8–1.8 nm, with $h_{max}$ = 1.0 ± 0.2 nm. Given that the AFM image of CYP11A1 monomer has $h_{max}$ = 1.6 ± 0.2, and that the masses of AdR monomer (Mr = 50 kDa) and CYP11A1 monomer (Mr = 58 kDa) are similar, it may well be suggested that the objects with the $h_{max}$ = 1.8 ± 0.2 nm correspond to AdR monomers. Bearing in mind that $Mr_{Ad}$ (13 kDa) < $Mr_{AdR}$ (50 kDa), it was inferred that the objects with the ρ(h) distribution maximum at $h_{max}$ = 1.0 ± 0.2 nm are Ad monomers.

The binary complexes were not AFM-registered in the (Ad + P450 11A1mon) mixture but formation of these complexes was registered by optical biosensor [84]. The absence of the AFM images of Ad-P450 11A1mon complexes may be explained by blockage, upon complex formation, of adhesion sites of proteins to mica.

The AFM images of binary complexes formed in the (AdR + Ad) and (AdR + P450 11A1) mixtures are represented in Fig. 4. The $(\rho(h)_{AdR+Ad})$ distribution of imaged objects in the (AdR + Ad) mixture and comparison of this distribution with the ρ(h) distributions of the individual proteins AdR and Ad reveals marked distinctions (Fig. 4). It can be seen that the $\rho(h)_{AdR+Ad}$ distribution is characterized by the increased number of objects with heights in the range 1.8–2.6 nm and the maximum height $h_{max}$ = 2.3 ± 0.2 nm — compared to distributions of individual proteins. The increase in the

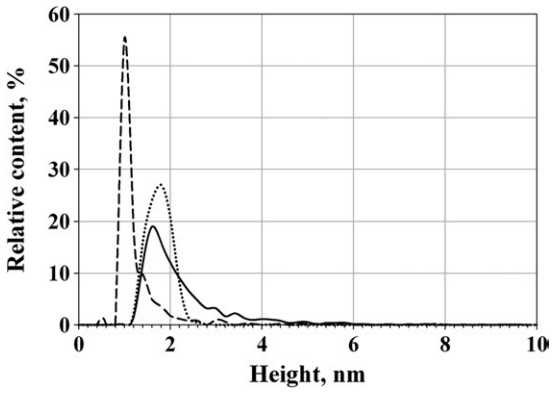


**Fig. 3.** Density of distribution with height ρ(h) of monomerized P450 11A1 (——), Ad (— — —) and AdR (·····). AFM tapping mode. Experimental conditions for monomerized P450 11A1 were the same as in Fig. 1, for Ad and AdR: 5 μl of 1 μM Ad and 5 μl of 1 μM AdR in 50 mM KP, pH 7.4, were deposited onto the freshly cleaved mica surface, and left for 2 min. Then each sample was rinsed with distilled water. T = 25 °C [84].

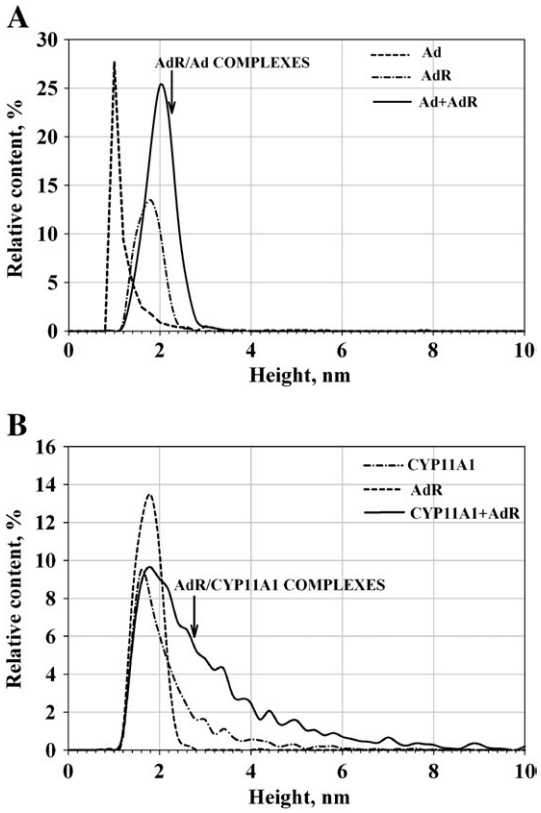


**Fig. 4.** Density of distribution with height ρ(h) of AFM images in the (AdR + Ad) mixture (——) vs. densities of distributions of Ad (- - -) and AdR (- • - • -) (A); in the (AdR + P450 11A1) mixture (_____) vs. AdR (- - -) and monomerized P450 11A1 (- • - • -) (B). AFM tapping mode. Experimental conditions: 10 μl mixture of 5 μM solutions of appropriate individual proteins in 50 mM KP, pH 7.4, was incubated for 10 min, diluted 2.5 times with the same buffer, and a 5-μl portion of the mixture was immediately placed onto mica and left for 3 min. Then each sample was rinsed with distilled water. T = 25 °C.T = 25 °C [84].

number of these new objects with the greater characteristic height is apparently due to formation in the (AdR + Ad) mixture of binary AdR/Ad complexes with $h_{max} = 2.3 \pm 0.2$ nm.

Similar situation was met for the imaged objects in the (AdR + P450 $11A1_{mon}$) mixture (Fig. 4). The spectrum of $\rho(h)_{AdR+CYP11A1}$ distributions in comparison with ρ(h) distributions of individual AdR and P450 $11A1_{mon}$ is characterized by the increase of additional objects in the distribution curve wing with heights in the range 2.2–6.0 nm and $h_{max} = 2.8. \pm 0.2$ nm. Based on these data, it was concluded that the increase in the number of these new objects with greater characteristic heights is due to formation of the binary AdR/CYP11A1 complexes with $h_{max} = 2.8. \pm 0.2$ nm.

To elucidate whether the ternary complexes were indeed formed in the P450 11A1 system, the AFM-imaged objects were obtained from the (AdR + Ad + P450 11A1) mixture and the ρ(h) distribution of these objects was compared to the distributions for the binary mixtures: $\rho(h)_{CYP11A1+Ad}$, $\rho(h)_{Ad+AdR}$, $\rho(h)_{AdR+CYP11A1}$ (Fig. 5). The (AdR + Ad + P450 11A1) mixture's distribution is characterized by the appearance of additional objects in the height range 2.8–7.0 nm with a broad maximum at $h_{max} = 4.0 \pm 1.0$ nm in the distribution curve wing compared to the distributions for binary mixtures. The proportion of these new objects with a great height in the (AdR + Ad + P450 11A1) mixture was (12 ± 4) %. Based on these data, it was concluded that the majority of objects with the distribution maximum at $h_{max} = 4.0 \pm 1.0$ nm are, in fact, the ternary CYP11A1/Ad/AdR complexes.

Thus, AFM enables to visualize individual membrane proteins and to register their binary and ternary complexes directly within the cytochrome P450 11A1 system — as was demonstrated for cytochromes P450 101 and P450 2B4 [40,41].

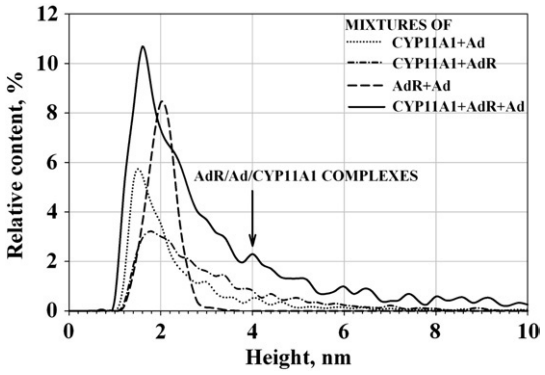


**Fig. 5.** Comparison of density of distribution ρ(h) of AFM images in the (AdR + Ad + CYP11A1) mixture (——) vs. $\rho(h)_{(CYP11A1+Ad)}$ (• • •), $\rho(h)_{(CYP11A1+AdR)}$ (- • - •- •) and $\rho(h)_{(AdR+Ad)}$ (- - - -) mixtures. AFM tapping mode. Experimental conditions were: 10 μl mixture of 7.5 μM solutions of appropriate individual proteins (CYP11A1 monomeric, containing 1.5% Emulgen 913, Ad and AdR) in 50 mM KP, pH 7.4, was incubated for 10 min, diluted 2.5 times in the same buffer, and a 5-μl portion of the mixture was immediately placed onto mica and left for 3 min. Then each sample was rinsed with distilled water. T = 25 °C. [84].

### *2.3.2. OB in studies of the P450 11A1 system*

Formation of binary (Ad/PdR, Ad/P450 11A1 and AdR/P450 11A1) complexes in oxidation conditions was registered by OB-RM [85] upon Ad immobilization and did not occur upon Ad immobilization in this system [12,80]. This was taken to mean that the positively charged amino acid residues of AdR and P450 11A1 are absolutely necessary for their complexation with Ad. The lifetimes of Ad/AdR and Ad/P450scc were measured and are represented in Table 1. The values of these lifetimes are similar to these obtained by Schiffeler at al. with OB based on SPR [71]. Comparison of the lifetime $\tau_{LT}$ of binary (Ad/AdR and Ad/P450 11A1) complexes with the time required for a single hydroxylation cycle $\tau_{cat} = 1/kcat$ has shown that the lifetimes of these complexes are longer by an order than the time required for a single hydroxylation cycle. To elucidate the influence of proteins' oxidation state on their interaction kinetics, additional measurements of $k_{on}$ and $k_{off}$ constants were conducted; also, the values of $K_D$ and $\tau_{LT}$ – in both the oxidation and hydroxylation conditions – were determined [12,80]. Table 1 presents the data calculated from the kinetic curves of $k_{on}$, $k_{off}$, $\tau_{LT}$ and $K_D$ for the complex formation reaction in these pairs in both conditions. The obtained results are shown in Table 1. One can see that the difference in kinetic parameters for hydroxylation and oxidation conditions is only revealed for the binary Adim/P450 11A1 complexes [$\tau_{LT}$ (*HYD*) is 125 ± 30 s but $\tau_{LT}$ (*OX*) is 900 ± 80]. The lifetimes of Ad/AdR complexes were $\tau_{LT} = 500 \pm 175$ s (*HYD*) and $\tau_{LT} = 286 \pm 123$ s (*OX*). Analysis of literature data reveals the scatter in $\tau_{cat}$ values for P450 11A1: from 2 s to 100 s [4,86] depending on experimental conditions used. In hydroxylation conditions realized in this study, $\tau_{cat}$ is about 25 s [12,80]. Comparing $\tau_{LT}$ (*HYD*) with $\tau_{cat}$ for all binary complexes (excluding P450 11A1/AdR whose $\tau_{LT} = 10$–40 s is practically equal to $\tau_{cat}$) one may conclude that the binary complexes formed are ineffective. It is well known that direct electron transfer from AdR to P450 11A1 does not exist [4]. That means that for hydroxylation of cholesterol to occur it is necessary to bind Ad to the binary AdR/P450 11A1 complex. This will allow the binary complex to be turned into the ternary one, which is impossible for the shuttle model. Calculation of productivity of binary Ad/AdR and Ad/P450 11A1 complexes according Eq. (3) (at n = 6, where 6 is a number of electrons necessary for cholesterol side chain cleavage [4]) have demonstrated that productivity of binary Ad/AdR and Ad/P450 11A1 complexes does not exceed 3%, i.e. the binary complexes here considered are practically non-productive.

Formation of OB-registered ternary AdR/Ad/P450 11A1 complexes was discussed [11,85]. It was shown that the lifetime of ternary complexes obtained in oxidation conditions exceeds the time required

for completion of a single hydroxylation cycle [11,85]. The experiments aimed at revelation of ternary complexes within the P450 11A1-containing system in hydroxylation conditions were conducted by addition of Ad to $AdR_{im}$ in the presence of P450 11A1 in the incubation mixture containing: 50 mM KP (pH 7.4), 150 mM KCl, 5 mM NADPH and 10 μM cholesterol [12,80]. The data obtained in these experiments are indicative of formation of the ternary AdRim/P450 11A1/Ad complexes in both the hydroxylation and oxidation conditions. The lifetime of a complex thus formed makes up $\tau_{LT} = 25 \pm 13$ s in both conditions. Comparison of the ternary AdR/Ad/P450 11A1 complex lifetime ($\tau_{LT} = 25 \pm 13$ s) with the time required for the cholesterol side chain cleavage ($\tau_{cat}$ ~25 s) shows that the $\tau_{LT}/\tau_{cat}$ ratio is equal to 1 and, hence, during the ternary complex lifetime 1 hydroxylation cycle in one ternary complex can be realized. Therefore, all the ternary AdR/Ad/P450 11A1 complexes formed within the P450 11A1 system in hydroxylation conditions may be considered as productive.

Thus, AFM is able to register and visualize isolated proteins, binary and ternary complexes within the P450 11A1 system while OB-RM is able to measure kinetic contents of complex formation process and establish the productivity of ternary AdR/Ad/P450 11A1 and non-productivity of binary Ad/AdR and Ad/P450 11A1 complexes.

Summarizing the data obtained in AFM and OB studies of the three multiprotein P450 systems the following conclusions may be made. AFM allows to register formation of binary and ternary protein complexes in all the three P450101, P450 11A1 and P4502B4-containing monooxygenase systems. OB enables kinetically characterize complex formation of these proteins and measure their lifetime. Comparison of the complexes' lifetime with the single catalytical cycle time of each enzymatic system allowed to choose its more preferable functioning model. As is known, there are two models for the functioning of the P450101 and P450 11A1 systems: the shuttle mechanism [74,75] and the cluster model [76] based on ternary complex formation. In realization of the shuttle mechanism, the binary complex is productive on condition that $\tau_{LT} < \tau_{cat.}$ If $\tau_{LT} >> \tau_{cat,}$ then the binary complex is non-productive as was effectively demonstrated previously for PdR/Pd or Pd/P450101 in the P450101 system and for AdR/Ad or Ad/P450 11A1 in the P450 11A1 system. If the mechanism is described through formation of ternary complexes and the ternary complex lifetime $\tau_{LT} \geq \tau_{cat}$, then these complexes are productive as was shown for the case with PdR/Pd/P450101 complexes in the P450101 system and with AdR/Ad/P450 11A1 complexes in the P450 11A1 system. It appears therefore that the mechanism of functioning of these two systems is apparently realized through ternary complexes and not by the shuttle mechanism. In case of the P450 2B4 system, all its binary complexes (Fp/2B4 and b5/2B4) as well as its ternary (Fp/2B4/b5) complexes are productive because the lifetime of each such complex is sufficient to permit completion of one hydroxylation cycle.

## Acknowledgements

We express gratitude to Dr. Galina P. Kuznetsova and Dr. Natalia F. Semenkova for protein isolation and purification.

This work was supported by the Russian Foundation for Basic Research (RFBR) Grants # 09-04-12113 OFR-m and by the Ministry of Educ. and Sci. Contract 02.740.11.0791.

## References

[1] R. Neeli, H.M. Girvan, A. Lawrence, M.J. Warren, D. Leys, N.S. Scrutton, A.W. Munro, The dimeric form of flavocytochrome P450BM3 is catalytically functional as fatty acid hydroxylase, FEBS Lett. 579 (2005) 5582–5588.
[2] T. Omura, Structural diversity of cytochrome P450enzyme system, J. Biochem. 147 (2010) 297–306.
[3] Ortiz de Montellano, Cytochrome P450: Structure, Mechanism, and Biochemistry, 3rd EdCluvwer Academic/Plenum Publishers, New York, 2005.
[4] A.I. Archakov, G.I. Bachmanova, Cytochrome P450 and Active Oxygen, Taylor&-Francis, London, New York, Philadelphia, 1990.
[5] R. Bernhardt, Cytochrome P450: structure, function, and generation of reactive oxygen species, Rev. Physiol. Biochem. Pharmacol. Volume 127 (1996) 137–221.
[6] David F.V. Lewis, Guide to Cytochromes P450. Structure and Function, Taylor & Francis, London and New York, 2001.
[7] N.C. Gerber, S.G. Sligar, A role for Asp-251 in cytochrome P450cam oxygen activation, J. Biol. Chem. 269 (1994) 4260–4266.
[8] E. Szczesna-Skorupa, B. Mallah, B. Kemper, Fluorescence resonance energy transfer analysis of cytochromes P450 2C2 and 2E1 molecular interactions in living cells, J. Biol. Chem. 278 (2003) 31269–31276.
[9] V. Shumyantseva, E. Suprun, T. Bulko, A. Archakov, Electrochemical methods for the investigation of bioaffinity interactions based on gold nanoparticles modified sensors, Electroanalysis 21 (2009) 530–535.
[10] Hanukoglu, V. Spitsberg, J.A. Bumpus, K.M. Dus, C.R. Jefcoate, Adrenal mitochondrial cytochrome P-450scc, cholesterol and adrenodoxin interactions at equilibrium and during turnover, J. Biol. Chem. 256 (1981) 4321–4328.
[11] Yu.D. Ivanov, I.P. Kanaeva, I.I. Karyzina, S.A. Usanov, G. Hui Bon Hoa, S.G. Sligar, A.I. Archakov, Revelation of ternary complexes between redox partners in cytochrome P450-containing monooxygenase systems by the optical biosensor method, J. Inorg. Biochem. 87 (2001) 175–184.
[12] Yu. Ivanov, A.V. Ivanov, A.L. Kaysheva, V.G. Zgoda, S.A. Usanov, G. Hui Bon Hoa, A.I. Archakov, Productive and non-productive complexes in cytochrome P450-containing systems, Biomed. Khim. (Moscow) 55 (2009) 310–330.
[13] T.L. Poulos, B.C. Finzel, I.C. Gunsalus, G.C. Wagner, J. Kraut, The 2.6 A crystal structure of *Pseudomonas putida* cytochrome P450, J. Biol. Chem. 260 (1985) 16122–16130.
[14] T.C. Pochapsky, X.M. Ye, G. Ratnaswamy, T.A. Lyons, An NMR-derived model for the solution structure of oxidized putidaredoxin, a 2-Fe, 2-S ferredoxin from *Pseudomonas*, Biochemistry 33 (1994) 6424–6432.
[15] I.R. Sevrioukova, C. Garcia, H. Li, B. Bhaskar, T.L. Poulos, Crystal structure of putidaredoxin, the [2Fe–2S] component of the P450cam monooxygenase system from *Pseudomonas putida*, J. Mol. Biol. 333 (2003) 377–392.
[16] E.E. Scott, Y.A. He, M.R. Wester, M.A. White, C.C. Chin, J.R. Halpert, E.F. Johnson, C.D. Stout, An open conformation of mammalian cytochrome P450 2B4 at 1.6-Å resolution, PNAS 100 (2003) 13196–13201.
[17] M. Wang, D.L. Roberts, R. Paschke, T.M. Shea, B.S.S. Masters, J.P. Kim, Three-dimensional structure of NADPH-cytochrome P450 reductase: prototype for FMN- and FAD-containing enzymes, Proc. Natl Acad. Sci. USA 94 (1997) 8411–8416.
[18] M.J. Rodriguez-Maranon, F. Qiu, R.E. Stark, S.P. White, X. Zhang, S.I. Foundling, V. Rodriguez, C.L. Schilling 3rd, R.A. Bunce, M. Rivera, $^{13}C$ NMR spectroscopic and X-ray crystallographic study of the role played by mitochondrial cytochrome $b_5$ heme, Biochemistry 17 (35) (1996) 16378–16390.
[19] I.A. Pikuleva, K. Tesh, M.R. Waterman, Y. Kim, The tetriary structure of full-length bovine adrenodoxin suggests functional dimers, Arch. Biochem. Biophys. 373 (2000) 44–55.
[20] G.A. Ziegler, C. Vonrhein, I. Hanukoglu, G.E. Schulz, The structure of adrenodoxin reductase of mitochondrial P450 systems: electron transfer for steroid biosynthesis, J. Mol. Biol. 289 (1999) 981–990.
[21] T.H. Bayburt, S.G. Sligar, Single-molecule height measurements on microsomal cytochrome P450 in nanometer-scale phospholipid bilayer disks, Proc. Natl Acad. Sci. USA 99 (2002) 6725–6730.
[22] O.I. Kiselyova, O.L. Gur'ev, A.V. Krivosheev, S.A. Usanov, I.V. Yaminsky, Atomic force microscopy studies of Langmuir–Blodgett films of cytochrome P450 scc (CYP11J1): hemoprotein aggregation states and interaction with lipids, Langmuir 15 (1999) 1353–1360.
[23] A. Philippsen, W. Im, A. Engel, T. Schirmer, B. Roux, D.J. Muller, Imaging the electrostatic potential of transmembrane channels: atomic probe microscopy of OmpF porin, Biophys. J. 82 (2002) 1667–1676.
[24] F. Moreno-Gerrero, J. Colchero, J. Gomez-Herrero, A.M. Baro, Atomic force microscopy contact, tapping and jumping modes for imaging biological samples in liquids, Phys. Rev. E 69 (2004) 031915-1-0319159.
[25] P.K. Hansma, J.P. Cleveland, M. Radmacher, D.A. Walters, P.E. Hillner, M. Bezanilla, M. Fritz, D. Vie, H.G. Hansma, Tapping mode atomic force microscopy in liquids, Appl. Phys. Lett. 64 (1994) 1738–1740.
[26] Y.F. Dufrene, Using nanotechniques to explore microbial surfaces, Nat. Rev. Microbiol. 2 (2004) 51–460.
[27] Y.G. Kuznetsov, A. Low, H. Fan, A. McPherson, Atomic force microscopy investigation of isolated virions of murine leukemia virus, J. Virol. 79 (2005) 1970–1974.
[28] Yu.D. Ivanov, V.F. Uchaykin, T.O. Pleshakova, A.I. Archakov, Creation of new bioimmunosensors and biochips for infection and nonifection diseases. Atomic force biochips for hepatitis C diagnostics, Physiol. Pathol. Immune Syst. (Rus) 10 (2006) 11–14.
[29] Yu.D. Ivanov, P.A. Frantsuzov, T.O. Pleshakova, V.S. Ziborov, S.K. Svetlov, N.I. Krohin, V.A. Konev, O.B. Kovalev, V.F. Uchaikin, O.N. Yastrebova, P.G. Sveshnikov, A.I. Archakov, Atomic force microscopy of serological markers of viral hepatites B and C, Biomed. Khim. 55 (2000) 689–701.
[30] M. Plomp, M.K. Rice, E.K. Wagner, A. McPherson, A.J. Malkin, Rapid visualization at high resolution atomic force microscopy: structural studies of herpes simplex virus-1, Am. J. Pathol. 160 (2002) 1959–1966.
[31] S.R. Nettikadan, J.C. Johnson, C. Mosher, E. Henderson, Virus particle detection by solid phase immunocapture and atomic force microscopy, Biochem. Biophys. Res. Commun. 311 (2) (2003) 540–545.
[32] D.V. Klinov, L.P. Martynkina, V.Yu. Yurchenko, V.V. Demin, S.A. Streltsov, Yu.A. Gerasimov, Yu. Yu, Vengerov effect of supporting substrates on the structure of DNA and DNA–trivaline complexes studied by atomic force microscopy, Russ. J. Bioorg. Chem. 29 (4) (2003) 363–367.

[33] A.I. Archakov, Y.D. Ivanov, A.V. Lisitsa, V.G. Zgoda, AFM fishing nanotechnology is the way to reverse the Avogadro number in proteomics, Proteomics 7 (2007) 4–9.
[34] A.I. Archakov, Y.D. Ivanov, A.V. Lisitsa, V.G. Zgoda, Biospecific irreversible fishing coupled with atomic force microscopy for detection of extremely low-abundant proteins, Proteomics 9 (2009) 1326–1343.
[35] C. Bustamante, J. Vesenka, C.L. Tang, W. Rees, M. Guthod, R. Keller, Circular DNA molecules imaged in air by scanning force microscopy, Biochemsistry 31 (1992) 22–26.
[36] J. Huff, M.P. Lynch, S. Nettikadan, J.C. Johnson, et al., Label-free protein and pathogen detection using the atomic force microscopy, J. Biol. Screening 9 (2004) 491–497.
[37] A. Ramacviciene, V. Snitka, R. Mieliauskiene, A. Ramanavicius, AFM study of complement system assembly initiated by antigen-antibody complex, Cent. Eur. J. Chem. 4 (1) (2006) 194–206.
[38] N.V. Medvedeva, O.M. Ipatova, Yu.D. Ivanov, A.I. Drozhzhin, A.I. Archakov, Nanobiotechnology and nanomedicine, Biomed. Khim. 52 (2006) 529–546.
[39] O.I. Kiselyova, I.V. Yaminsky, Yu.D. Ivanov, I.P. Kanaeva, V.Yu. Kuznetsov, A.I. Archakov, AFM study of membrane proteins, cytochrome P450 2B4 and NADPH-cytochrome P450 reductase, and of their complex formation, Arch. Biochem. Biophys. 371 (1999) 1–7.
[40] V.Yu. Kuznetsov, Yu.D. Ivanov, V.A. Bykov, S.A. Saunin, I.A. Fedorov, S.V. Lemeshko, G.H. Bon-Hoa, A.I. Archakov, Atomic force microscopy detection of molecular complexes in multiprotein P450cam containing monooxygenase system, Proteomics 2 (2002) 1699–1705.
[41] V.Yu. Kuznetsov, Yu.D. Ivanov, A.I. Archakov, Atomic force microscopy revelation of molecular complexes in the multiprotein cytochrome P450 2B4-containing system, Proteomics 4 (2004) 2390–2396.
[42] Y.D. Ivanov, P.A. Frantsuzov, V.A. Bykov, S.P. Besedin, Gaston Hui Bon Hoa, A.I. Archakov, Comparative investigation of PdR by usual and ultrafine atomic force microscopy, Anal. Methods 2 (2010) 688–693.
[43] D.G. Myszka, R.L. Rich, SPR's high impact on drug discovery: resolution, throughput and versatility, Drug Discovery World Spring, 2003, pp. 49–55.
[44] P. Englebienne, A. Van Hoonacker, M. Verhas, Surface plasmon resonance: principles, methods and applications in biomedical sciences, Spectroscopy 17 (2003) 255–273.
[45] J.S. Yuk, K.-S. Ha, Proteomics application of SPR biosensors: analysis of protein array, Exp. Mol. Med. 37 (2005) 1–10.
[46] A.I. Archakov, Y.D. Ivanov, Optical biosensor and scanning probe microscopy studies of cytochrome P450 interactions with redox partners and phospholipid layers, Methods Enzymol. 357 (2002) 94–103.
[47] Y.D. Ivanov, O.V. Gnedenko, L.I. Nikolaeva, V.A. Konev, O.B. Kovalev, V.F. Uchaikin, V. M. Govorun, V.I. Pokrovsky, A.I. Archakov, Detection of hepatitis B virus surface antigen with the use of an optical biosensor, Zh. Microb. (Moscow) 2 (2003) 58–62.
[48] O.A. Buneeva, O.V. Gnedenko, N.G. Panova, M.V. Medvedeva, Yu.D. Ivanov, A.E. Medvedev, Glycerol-3-phosphate dehydrogenase is a cytosolic isatin-binding protein, Biomed. Khim. 49 (2003) 627–631.
[49] A.V. Veselovsky, Yu.D. Ivanov, A.S. Ivanov, A.I. Archakov, P. Lewi, P. Janssen, Protein–protein interactions: mechanisms and modification by drugs, J. Mol. Recognit. 15 (2002) 405–422.
[50] A.I. Archakov, V.M. Govorun, A.V. Dubanov, Y.D. Ivanov, A.V. Veselovsky, P. Lewi, P. Janssen, Protein–protein interactions as a target for drugs in proteomics, Proteomics 3 (2003) 380–391.
[51] N.I. Rachenkova, Yu.D. Ivanov, V.S. Scvorcov, A.S. Ivanov, A.A. Molnar, G.H. Bon-Hoa, A.I. Archakov, Optical biosensors study and molecular modeling of interactions between cytochrome P450cam and cytochrome b5, Biomed. Khim. 51 (2005) 501–512.
[52] Y.D. Ivanov, V.M. Govorun, V.A. Bykov, A.I. Archakov, Nanotechnologies in proteomics, Proteomics 5 (2006) 1399–1414.
[53] A.I. Archakov, Yu.D. Inanov, in: Nanotechnology and the Health of the EU Citizen in 2020. 2005 Edinburg, UK www.euronanoforum2005.org.
[54] N.I. Rachenkova, Yu.D. Ivanov, A.A. Molnar, A.I. Archakov, Optical biosensor study interaction between trypsin and trypsin inhibitor, Biomed. Khim. 51 (2005) 614–623.
[55] A. Medvedev, O. Buneeva, O. Gnedenko, V. Fedchenko, M. Medvedeva, Y. Ivanov, V. Glover, M. Sandler, Isatin interaction with glyceraldehyde-3-phosphate dehydrogenase, a putative target of neuroprotective drugs: partial agonism with deprenyl, Neural Transm. 71 (2006) 97–103.
[56] A.I. Archakov, Yu.D. Ivanov, Analytical nanobiotechnology for medicine diagnostics, Mol. Biosyst. 3 (2007) 336–342.
[57] V.V. Koval, O.V. Gnedenko, Yu.D. Ivanov, O.S. Fedorova, A.I. Archakov, D.G. Knorre, Real-time oligonucleotide hybridization kinetics monitored by resonant mirror technique, IUBMB Life 48 (1999) 317–320.
[58] Yu.D. Ivanov, N.G. Panova, O.V. Gnedenko, O.A. Buneeva, A.E. Medvedev, A.I. Archakov, The study of tissue and subcellular distribution of isatin binding proteins by means if optical biosensor technique, Vopr. Med. Khim. 48 (2002) 73–83.
[59] Yu.D. Ivanov, O.V. Gnedenko, V.A. Konev, O.B. Kovalev, L.I. Nikolaeva, N.V. Semenova, V.F. Uchaikin, A.I. Archakov, The optical biosensor technique for detection of hepatitis B virus surface antigen, Vopr. Med. Khim. 47 (2001) 419–425.
[60] D.A. Dmitriev, Y.S. Massino, O.L. Segal, M.B. Smirnova, E.V. Pavlova, G.I. Kolyaskina, K.G. Gurevich, O.V. Gnedenko, Yu.D. Ivanov, A.I. Archakov, A.P. Osipov, A.D. Dmitriev, A.M. Egorov, Analysis of bispecific monoclonal antibody binding to immobilized antigens using an optical biosensor, Biochemistry (Moscow) 67 (2002) 1356–1365.
[61] D.A. Dmitriev, Y.S. Massino, O.L. Segal, M.B. Smirnova, E.V. Pavlova, K.G. Gurevich, O.V. Gnedenko, Y.D. Ivanov, G.I. Kolyaskina, A.I. Archakov, A.P. Osipov, A.D. Dmitriev, A.M. Egorov, Analysis of the binding of bispecific monoclonal antibodies with immobilized antigens (human IgG and horseradish peroxidase) using a resonant mirror biosensor, J. Immunol. Methods 261 (2002) 103–118.
[62] K. Sigmundsson, G. Masson, R. Rice, N. Beaucheimin, B. Obrink, Determination of active concentrations and association/dissociation rate constants of interacting biomolecules: an analytical solution to the theory for kinetic and mass transport limitations in biosensor technology and its experimental verification, Biochemistry 41 (26) (2002) 8263–8276.
[63] J. Homola, S.S. Yee, G. Gauglitz, Surface plasmon resonance sensors: review, Sens. Actuators, B 54 (1999) 3–15.
[64] J.M. Brockman, B.P. Nelson, R.M. Corn, Surface plasmon resonance imaging measurements of a ultrathin organic films, Ann. Rev. Phys. Chem. 51 (2000) 41–63.
[65] J.S. Yuk, K.-S. Ha, Proteomics application of SPR biosensors: analysis of protein array, Exp. Mol. Med. 37 (2005) 1–10.
[66] D. Yeung, A. Gill, C.H. Maule, R.J. Davies, Detection and quantification of biomolecular interactions with optical biosensors, Trends Anal. Chem. 14 (1995) 49–56.
[67] U. Jonsson, L. Fagerstam, B. Ivarsson, B. Johnsson, Real time biospecific interaction analysis using surface plasmon resonance and a sensor chip technology, Biotechniques 11 (1991) 620–627.
[68] R.L. Rich, D.G. Myszka, Survey of the year 2006 commercial optical biosensor literature, J. Mol. Recognit. 20 (2007) 300–366.
[69] R. Cush, J.M. Cronin, W.J. Stewart, C.H. Maule, J. Molloy, N.J. Goddard, The resonant mirror: a novel optical biosensor for direct sensing of biomolecular interactions part I: principle of operation and associated instrumentation, Biosens. Bioelectron. 8 (1993) 347–354.
[70] H. Vaisocherova, J. Homola SPR, Biosensors for medical diagnostics, Springer Ser. Chem. Sens. Biosens. 4 (2006) 229–247.
[71] B. Schiffler, A. Zollner, R. Bernhardt, Stripping down the mitochondrial cholesterol hydroxylase system, a kinetic study, J. Biol. Chem. 279 (2004) 32269–34276.
[72] Yu.D. Ivanov, I.P. Kanaeva, V.Yu. Kuznetsov, M. Lehnerer, J. Schulze, P. Hlavica, A.I. Archakov, The optical biosensor studies on the role of hydrophobic tails of NADPH-cytochrome P450 reductase and cytochromes P450 2B4 and b5 upon productive complex formation within a monomeric reconstituted system, Arch. Biochem. Biophys. 362 (1999) 87–93.
[73] S. Way, B. Hill, Methods Guide for IAsys plus and IAsys Auto+. Affinity Sensors, Human-Computer Interface Limited, Cambridge, England, 1996.
[74] J.D. Lambeth, L.M. Geren, F. Millet, Adrenodoxin interaction with adrenodoxin reductase and cytochrome P-450scc. Cross-linking of protein complexes and effects of adrenodoxin modification by 1-ethyl-3-(3-dimethylaminopropyl) carbodiimide, J. Biol. Chem. 259 (1984) 10025–10029.
[75] L. Geren, J. Tuls, P.O. Brien, F. Millett, J.A. Peterson, The involvement of carboxylate groups of putidaredoxin in the reaction with putidaredoxin reductase, J. Biol. Chem. 261 (1986) 15491–15495.
[76] T. Kido, T.J. Kimura, The formation of binary and ternary complexes of cytochrome $P\text{-}450_{scc}$ with adrenodoxin and adrenodoxin reductase–adrenodoxin complex. The implication in ACTH function, Biol. Chem. 254 (1979) 11806–11815.
[77] R. Guckenberger, M. Heim, G. Cevc, H.F. Knapp, W. Wiegrabe, A. Hillebrand, Scanning tunneling microscopy of insulators and biological specimens based on lateral conductivity of ultrathin water films, Science 266 (1994) 1538–1540.
[78] Yu.D. Ivanov, I.P. Kanaeva, I.P. Karuzina, A.I. Archakov, G. Bon-Hoa, S.G. Sligar, Molecular recognition in the P450cam monooxygenase system: direct monitoring of protein–protein interaction by using optical biosensor, Arch. Biochem. Biophys. 391 (2001) 255–264.
[79] M.J. Hintz, D.M. Mock, L.L. Peterson, K. Tuttle, J.A. Peterson, Equilibrium and kinetic studies of the interaction of cytochrome P-450cam and putidaredoxin, J. Biol. Chem. 257 (1982) 14324–14332.
[80] Yu. Ivanov, A.V. Ivanov, A.L. Kaysheva, V.G. Zgoda, S.A. Usanov, G. Hui Bon Hoa, A.I. Archakov, Productive and non-productive complexes in cytochrome P450-containing systems, Biochemistry (Moscow) 3 (2009) 183–197.
[81] E.J. Mueller, P.J. Loida, S.G. Sligar, in: P.R. Ortiz De Montellano (Ed.), Cytochrome P450: Structure, Mechanism, and Biochemistry, 2nd Ed, Plenum Press, New York, 1995, p. 103, Chap. 3.
[82] I.P. Kanaeva, E.D. Skotselyas, G.P. Kuznetsova, G.N. Antonova, Reconstruction of a membrane monooxygenase cytochrome P 450-containing system in the liver using detergents in solution, Biochemistry-USSR 50 (1985) 1382–1388.
[83] Yu.D. Ivanov, I.P. Kanaeva, M.A. Eldarov, K.G. Skryabin, M. Lehnerer, J. Schulze, P. Hlavica, A.I. Archakov, The optical biosensor study of the parameters and role of hydrophobic tails of cytochrome P450 cytochromes P450 2B4, b5 and NADPH-flavoprotein in complex, Biochem. Mol. Biol. Int. 42 (1997) 731–737.
[84] Y.D. Ivanov, P.A. Frantsuzov, A. Zöllner, N.V. Medvedeva, A.I. Archakov, W. Reinle, R. Bernhardt, Atomic Force Microscopy Study of Protein–Protein Interactions in the Cytochrome CYP11A1 (P450scc)-Containing Steroid Hydroxylase System, Nanoscale Res. Lett. (2010), doi:10.1007/s11671-010-9809-5.
[85] Yu.D. Ivanov, S.A. Usanov, A.I. Archakov, The optical biosensor studies on the productive complex formation between the components of cytochrome P450scc dependent monooxygenase system, Biochem. Mol. Biol. Int. 47 (1999) 327–336.
[86] B. Schiffler, M. Kiefer, A. Wilken, F. Hannemann, H.W. Adolph, R. Bernhardt, The interaction of bovine adrenodoxin with CYP11A1 (cytochrome P450scc) and CYP11B1 (cytochrome P450 11β), J. Biol. Chem. 276 (2001) 36225–36232.